Structure *14*, 217–224, February 2006 ©2006 Elsevier Ltd All rights reserved DOI 10.1016/j.str.2005.10.013

Flexibility of Thiamine Diphosphate Revealed by Kinetic Crystallographic Studies of the Reaction of Pyruvate-Ferredoxin Oxidoreductase with Pyruvate

Christine Cavazza,[1,4,7] Carlos Contreras-Martel,[1,4,7,8] Laetitia Pieulle,[2,5] Eric Chabrière,[3,6] E. Claude Hatchikian,[2,5] and Juan C. Fontecilla-Camps[1,4,*]

[1] Laboratoire de Cristallographie et Cristallogenèse des Protéines
Institut de Biologie Structurale "Jean-Pierre Ebel"
CEA, UJF, CNRS
41 rue Jules Horowitz
38027 Grenoble Cedex 1
France

[2] Unité de Bioenérgetique et Ingénierie des Protéines
Institut de Biologie Structurale et Microbiologie
CNRS
31 chemin J. Aiguier
13402 Marseille Cedex 20
France

[3] Laboratoire de Cristallographie et Modélisation des Matériaux Minéraux et Biologiques
UMR 7036 CNRS, UHP
Nancy 1B.P. 239
54506 Vandoeuvre-les-Nancy
France

Summary

Pyruvate-ferredoxin oxidoreductases (PFOR) are unique among thiamine pyrophosphate (ThDP)-containing enzymes in giving rise to a rather stable cofactor-based free-radical species upon the decarboxylation of their first substrate, pyruvate. We have obtained snapshots of unreacted and partially reacted (probably as a tetrahedral intermediate) pyruvate-PFOR complexes at different time intervals. We conclude that pyruvate decarboxylation involves very limited substrate-to-product movements but a significant displacement of the thiazolium moiety of ThDP. In this respect, PFOR seems to differ substantially from other ThDP-containing enzymes, such as transketolase and pyruvate decarboxylase. In addition, exposure of PFOR to oxygen in the presence of pyruvate results in significant inhibition of catalytic activity, both in solution and in the crystals. Examination of the crystal structure of inhibited PFOR suggests that the loss of activity results from oxime formation at the 4′ amino substituent of the pyrimidine moiety of ThDP.

Introduction

In most organisms, pyruvate, a central component of intermediate metabolism, undergoes oxidative decarboxylation, a reaction that is coupled to the reduction of low-potential electron carriers and the subsequent generation of an energy-rich thioester bond between the nascent acyl group and coenzyme A (CoA). This reaction can be catalyzed either by the multienzyme complex pyruvate dehydrogenase (PDH) present in mitochondria and respiratory eubacteria with NAD as the electron acceptor (Patel and Roche, 1990; Reed, 1998) or by pyruvate:ferredoxin oxidoreductase (PFOR) (Kerscher and Oesterhelt, 1982) in anaerobic organisms, where electrons are transferred to acceptors with more negative potentials than NAD, such as ferredoxins (Fd). The corresponding reaction is:

$$CH_3\text{-}CO\text{-}COO^- + Fd_{ox} + CoA \leftrightarrow CH_3\text{-}CO\text{-}CoA + Fd_{red} + CO_2$$

PFOR, unlike PDH, is a metalloenzyme that contains three [4Fe-4S] clusters and can also carry out the reductive carboxylation of acetyl-CoA to yield pyruvate (Kerscher and Oesterhelt, 1982). This latter reaction is used by green photosynthetic and acetogenic bacteria (Evans et al., 1966) and by methanogens (Tersteegen et al., 1997) for CO_2 fixation. PFORs from different organisms vary in their oligomeric structures but are all phylogenetically closely related (Kletzin and Adams, 1996; Zhang et al., 1996). They are members of a large family of thiamine diphosphate (ThDP)-containing enzymes that are involved in both nonoxidative (for example, pyruvate decarboxylase and benzoyl-formate decarboxylase) and oxidative decarboxylations (pyruvate oxidase and PDH, in addition to PFOR). Transketolase (TK) is a related enzyme that transfers a ketol group from a ketosugar to an aldosugar.

The catalytic mechanism of ThDP-containing enzymes is considered to be dependent on the enzyme-bound cofactor adopting the "V" configuration that brings the 4′ amino group of the aminopyrimidine ring close to the C2 carbon of the thiazolium ring (Breslow, 1962) (Figure 1). It is widely accepted that hydrogen bonding of the carboxylate group from a glutamate residue to N1′ of the aminopyrimidine renders the 4′ position more basic through tautomerization to a 4′ imino species. A proton is subsequently extracted from C2, probably by the 4′ imino group (Schneider and Lindqvist, 1998), generating a carbanion adduct; the proton would then bind to the carbonyl oxygen of the substrate, facilitating the nucleophilic attack of the carbonyl carbon by the C2 carbanion. In the case of pyruvate, the formation of a tetrahedral species is followed by cleavage of the C1α-C2α bond and release of CO_2. Subsequent generation of the enamine (or the equivalent 2-α-carbanion) intermediate has been generally accepted. In PFORs, one of the two electrons involved in the reaction is transferred from the cofactor to a [4Fe-4S] cluster (Cammack et al., 1980; Menon and Ragsdale, 1997), thus generating an acetyl-ThDP radical species that, in the absence of CoA, can be very stable under anaerobic conditions. This is indeed the case for the homodimeric PFOR (M_r = 270,000 Da) from *Desulfovibrio africanus*, an anaerobic sulfate-reducing bacterium (Pieulle et al., 1995).

*Correspondence: juan.fontecilla@ibs.fr
[4] Lab address: http://www.ibs.fr/content/ibs/home/
[5] Lab address: http://bip.cnrs-mrs.fr/
[6] Lab address: http://www.lcm3b.uhp-nancy.fr/
[7] These authors contributed equally to this work.
[8] Present address: Laboratoire de Cristallographie Macromoléculaire, Institut de Biologie Structurale "Jean-Pierre Ebel," CEA, UJF, CNRS, 41, rue Jules Horowitz, 38027 Grenoble Cedex 1, France.

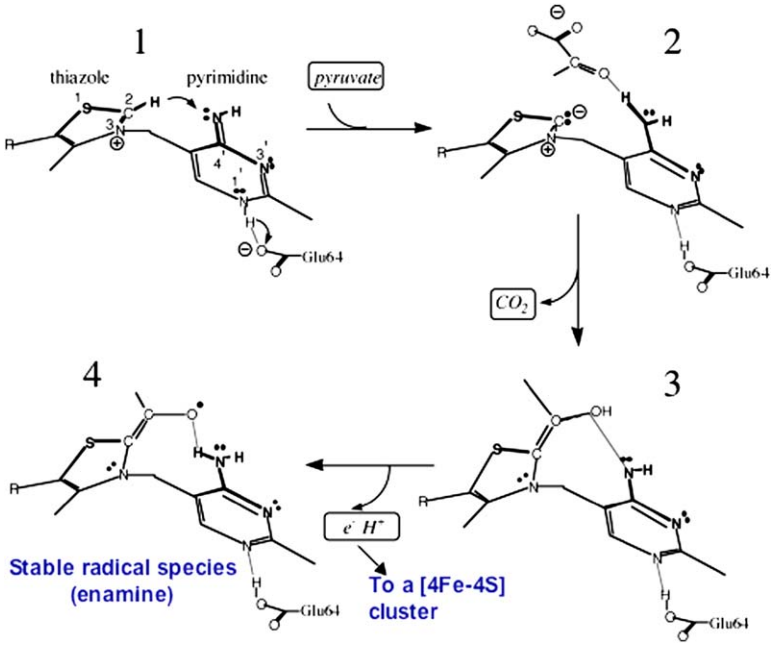

Figure 1. Standard Pyruvate Decarboxylation Cycle

(1) ThDP in the "V" conformation with an N4′ imino tautomer; (2) binding of pyruvate with its C2α facing the C2 carbanion of the thiazolium ring; (3) decarboxylation of the substrate and formation of the enamine species; and (4) formation of the free-radical species after one electron is transferred to one of the FeS clusters.

We have already reported the structures of the uncomplexed *D. africanus* PFOR at 2.3 Å resolution using crystals grown at pH 6.2 (Chabrière et al., 1999) and the 1.87 Å resolution active site structure of the putative free-radical form of PFOR solved from crystals soaked with pyruvate at pH 9.0 in an anaerobic glove box (Chabrière et al., 2001) (Protein Data Bank [PDB] codes 1b0p and 1kek, respectively). There are several surprising observations concerning the latter. First, the thiazole ring is puckered; second, the bond connecting the nascent acetyl group to this ring appears to be unusually long in our electron density maps (Bellvile et al., 1985; Gauld and Radom, 1997); and third, in our crystals the other product of the reaction, CO_2, remains tightly bound to the active site. Such tight binding is consistent with the reversibility of the reaction.

D. africanus PFOR crystals are remarkably stable with respect to pH. By moving away from pH 9.0, the optimal value for catalytic activity, we have been able to get snapshots of the reaction of the crystallized enzyme with pyruvate after different soaking times. In addition to these analyses, we report here the active site crystal structures of the native enzyme at 1.8 Å resolution and of an inhibited form of PFOR obtained through the modification of ThDP in the presence of air and pyruvate. These studies show that in PFOR the ThDP cofactor displays considerable conformational flexibility, a situation that is not likely to occur in other ThDP-containing enzymes.

Results

Structure and Solution Studies of the Oxygen-Inhibited Pyruvate-PFOR Complex

The inhibition of PFOR by incubation with pyruvate under aerobic conditions was first reported for *Trichomonas vaginalis* PFOR (Williams et al., 1990). Preincubation of *D. africanus* PFOR with pyruvate in an air-saturated buffer at 30°C also results in pyruvate-mediated inactivation of the enzyme (Table 1). The inhibition increased as the pyruvate concentration was raised from 0.1 mM to 5 mM. With higher concentrations (10–50 mM), a slight decrease of inhibition was observed. This is different from what was reported for *T. vaginalis* PFOR inhibition, which was almost completely abolished under similar conditions (Williams et al., 1990). The inactivation of *D. africanus* PFOR caused by pyruvate could be totally prevented by excluding air from the incubation buffer (data not shown). PFOR from dissolved crystals previously soaked overnight aerobically in an artificial mother liquor containing 50 mM pyruvate displayed only a residual activity of 0.26 ± 0.06 U/ml when tested using a standard assay (see Experimental Procedures). By comparison, PFORs from dissolved crystals soaked in the same solution under air but in the absence of substrate were activated after a few minutes with 9.67 ± 1.02 U/ml. Difference electron density maps indicated that the inhibited enzyme binds pyruvate and that the basis for inhibition appears to be a modification at the N4′ of the

Table 1. Inactivation of Pyruvate: Ferredoxin Oxidoreductase by Pyruvate in the Presence of Air

[Pyruvate] (mM)	Inhibition (%)
None	None
0.05	None
0.1	12.5
0.2	26.5
0.4	42
1	79.7
2.5	85.5
5	92.8
10	78.5
20	84.6
50	81.1

Each incubation contained pyruvate:ferredoxin oxidoreductase (2 units) in a final volume of 200 μl. The samples were incubated in air-saturated 50 mM Tris-HCl buffer (pH 8.5) for 60 min at 30°C, and a 1 μl sample was assayed for activity as described in Experimental Procedures.

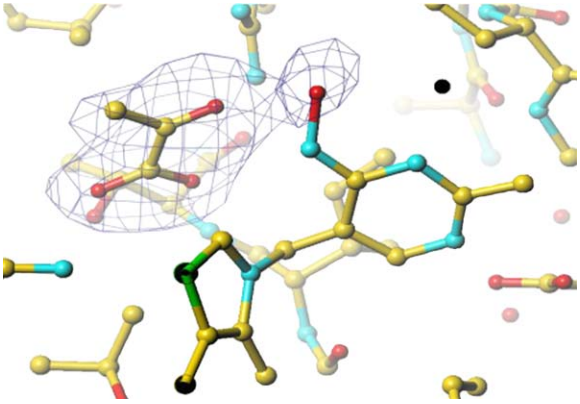

Figure 2. Electron Density Map of Oxygen-Inhibited PFOR

Pyruvate was excluded from phase and structure factor calculations (omit map). The electron density peak next to N4′ of the aminopyrimidine ring may represent the oxygen atom of an oxime moiety. This and the displacement of a water molecule are the only differences between inhibited and active PFORs (see Figure 3A). This figure and Figures 3 and 6 were prepared with TURBO (Roussel and Cambillaud, 1989).

aminopyrimidine ring of the ThDP cofactor (Figure 2). An electron density peak is found at a distance and angle that would be compatible with oxime formation. This modification displaces a water molecule found in the other PFOR structures. Although the loss of enzyme activity could also have arisen from damage to one or several of the three [4Fe-4S] clusters, examination of the final $[2F_o - F_c]$ electron density map did not reveal any unusual features around or at these centers (data not shown). Also, the results reported below concerning initial binding of pyruvate to active enzyme confirm that the inhibition observed here is not caused by a nonproductive substrate binding geometry.

Structure of the Native PFOR at 1.8 Å Resolution

It was possible to improve the resolution from the previously reported 2.3 Å structure (Chabrière et al., 1999) by growing crystals at 4ºC. The only significant difference between the two models is the identification in the latter of a putative chloride ion that occupies the binding pocket of CO_2 in the free-radical PFOR species and of the carboxylate group of pyruvate in the pyruvate-PFOR complexes described below (Figure 3, panel 1). Due to the rather limited resolution, the chloride ion was not detected in our previous 2.3 Å resolution analysis where the corresponding electron density was modeled as a water molecule (Chabrière et al., 1999). In retrospect, it makes sense that the pocket that binds the anionic carboxylate moiety can also bind a negative ion such as chloride.

Structures of Pyruvate-PFOR Complexes Obtained at Different Soaking Times under Anaerobic Conditions

As opposed to the original overnight soak carried out at pH 9.0 where PFOR activity is close to optimal and the radical species was obtained (Chabrière et al., 2001), the experiments reported here were done at pH 6.0 in order to significantly slow down the reaction (Figure 4). The observed lag phase is due to the slow activation of the enzyme by dithiothreitol (DTT) (Pieulle et al., 1995). The crystal flash-cooled at 100ºK after a 15 min soak (t_{15}) shows what appears to be mostly unreacted

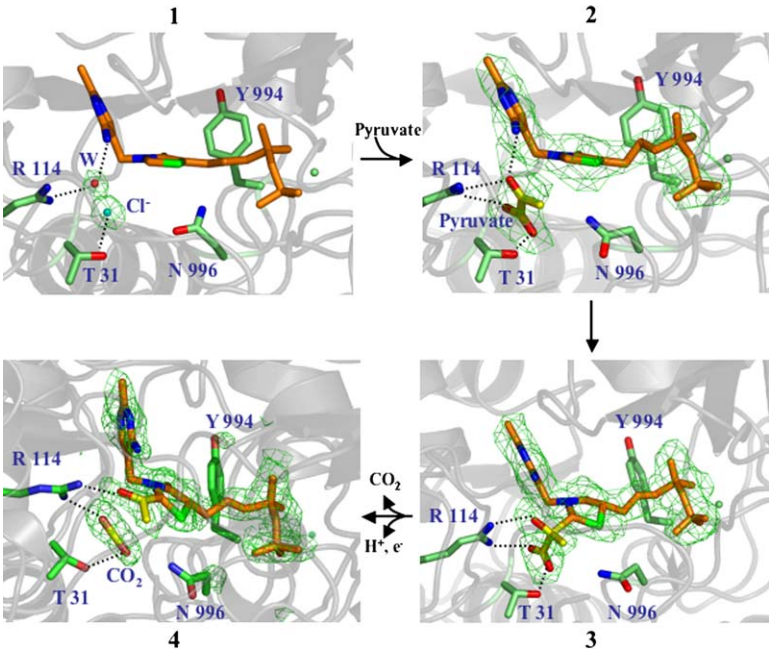

Figure 3. Omit Fourier Electron Density Maps around the Active Site of PFOR at Different Pyruvate Soak Times

(1) The active site of native PFOR at 1.8 Å resolution. The two electron density peaks contoured at 6 σ have been modeled as a chloride ion (Cl^-) and a water molecule (W). Averaged temperature factors for Cl^- and W are 21.2 $Å^2$ and 17.3 $Å^2$, respectively. The putative chloride ion occupies the site of both CO_2 in the radical species and the carboxylate group of unreacted pyruvate. (2) Electron density map of the pyruvate-PFOR complex after a 15 min soak in an artificial mother liquor solution containing 50 mM pyruvate and 25% (v/v) glycerol as cryoprotectant. Both ThDP and pyruvate have been excluded from phase and structure factor calculations. Under these conditions, the substrate binds productively but the reaction has not taken place to any observable degree (see Discussion). There is continuous electron density (contoured at the 1 σ level) between the carbonyl oxygen of the substrate and N4′ from the aminopyrimidine of ThDP, indicating a strong interaction between these two atoms. (3) Electron density map of the pyruvate-PFOR complex after a 40 min soak in an artificial mother liquor solution containing 50 mM pyruvate and 25% (v/v) glycerol as cryoprotectant. The map was calculated excluding atoms belonging to these moieties from phase and structure factor calculations. The observed electron density (contoured at the 3 σ level) has been interpreted as corresponding to the 2-(2-hydroxypropionyl)ethyl ThDP tetrahedral intermediate rather than a mixture of reacted and unreacted species (see Discussion). (4) The free-radical species. The map was calculated excluding atoms belonging to these moieties from phase and structure factor calculations. The conformation and bond lengths are essentially the same as in Chabrière et al. (2001).

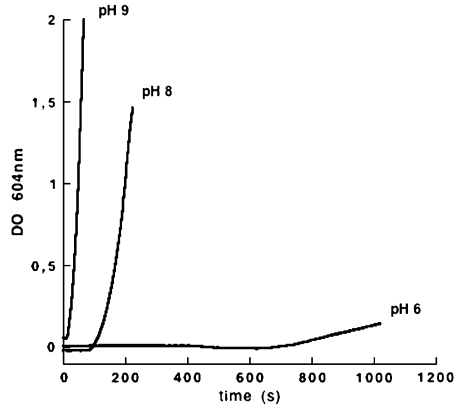

Figure 4. PFOR Activity Measurements as a Function of pH

We assign the long lag phase at acidic pH to the very sluggish activity of PFOR under these conditions. Because the as-isolated enzyme requires reductive activation, in the absence of added reductant, electrons probably come from pyruvate decarboxylation catalyzed initially by a small fraction of active PFOR. Subsequently, a cascade effect will accelerate the activation process. The decarboxylating reaction is much faster at optimal basic pHs, significantly reducing the lag time.

pyruvate bound exactly as in the oxygen-inhibited complex described above (Figure 3, panel 2). As expected under these conditions, the N4′ atom of the aminopyrimidine moiety of ThDP is not substituted but forms a hydrogen bond with a water molecule as in the native and free-radical species (Chabrière et al., 1999, 2001). The structure from a crystal that was soaked in a pyruvate solution for 40 min prior to flash cooling (t_{40}) shows electron density that can be interpreted as arising from a highly occupied tetrahedral reaction intermediate that forms prior to decarboxylation (see below and Figure 3, panel 3).

Figure 5 depicts the pairwise superposition of successive states as well as that of the initial (t_0) native form onto the t_{40} species, as determined in this study. Positive and negative difference electron density peaks obtained from a map calculated with ($F_{t40} - F_{t0}$) coefficients are also shown in the latter as indicators of conformational changes. These superpositions clearly illustrate the least motion, maximum overlap mechanism discussed, for instance, in the case of the related indolepyruvate decarboxylase (Schütz et al., 2005).

Composite Data Set

High doses of X-rays generate photoelectrons that could have modified the free-radical species detected in pyruvate-soaked PFOR crystals by electron paramagnetic resonance spectroscopy (Chabrière et al., 2001). Consequently, we collected a series of low-dose X-ray data sets and combined them to obtain a composite set (Berglund et al., 2002). Examination of the ($2F_o - F_c$) electron density map after refinement indicated that the conformation of the ThDP cofactor is not affected by exposure to high doses of X-rays (data not shown).

A Comparison of the Structures of the PFOR Free Radical and the Enamine Intermediate of the Related Enzyme TK

Fiedler et al. (2002) have reported the three-dimensional structure of TK from *Saccharomyces cerevisiae* reacted with hydroxypyruvate. A superposition of the substituted ThDP cofactors in TK and PFOR suggests that there is a major difference in the stereochemistry of their catalytic mechanisms (Figure 6). Whereas in TK neither the cofactor nor the protein undergo conformational changes upon enamine formation (Fiedler et al., 2002), in the free-radical form of PFOR, the thiazolium ring of ThDP approaches the tightly bound pyruvate molecule by shifting about 2 Å in its direction. This movement affects neither the aminopyrimidine ring nor the diphosphate moiety of ThDP which remain at their original positions. Both Tyr994 and Asn996 side chains rotate significantly upon reaction with pyruvate (Chabrière et al., 2001). Regardless of the detailed interpretation

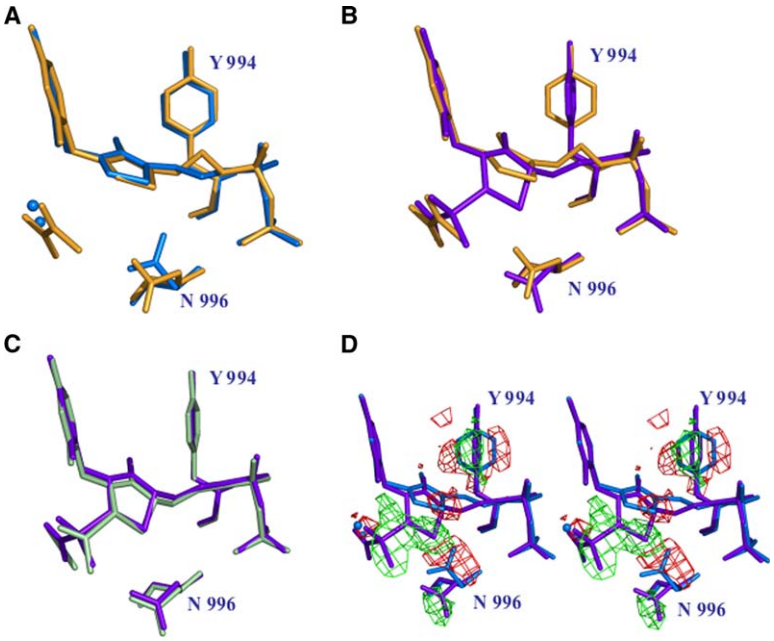

Figure 5. Pairwise Superposition of Successive States

(A) t_0 (blue) and t_{15} (gold) structures.
(B) t_{15} (gold) and t_{40} (violet) structures.
(C) t_{40} (violet) and free-radical (green) structures.
(D) Superposition of t_0 and t_{40} structures. Positive (green) and negative (red) difference electron density peaks obtained from a map calculated with ($F_{t40} - F_{t0}$) coefficients are also shown as indicators of conformational changes.

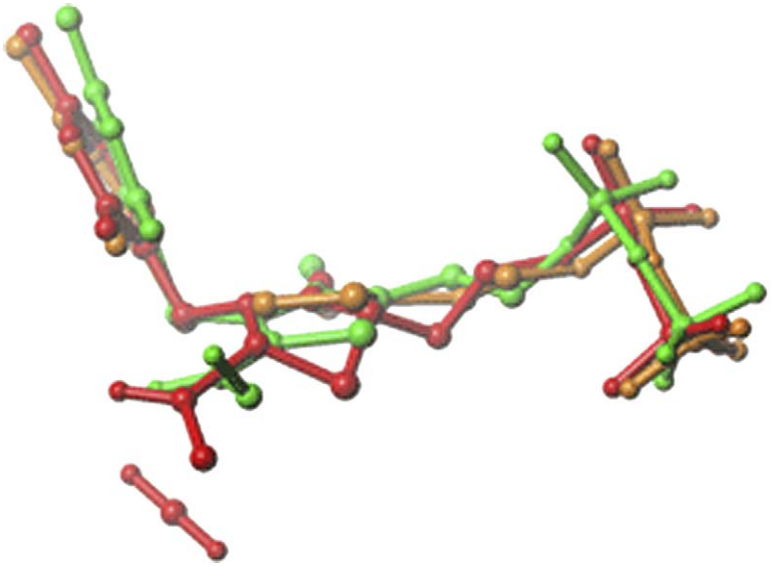

Figure 6. Superposition of the Enamine Species of TK and the Native and Putative Radical Forms of PFOR

In TK, the thiazole ring is found halfway between the two PFOR species. The relative positions of pyruvate and ThDP in PFOR make the formation of an enamine intermediate unlikely. Green, enamine species of TK; orange, native form of PFOR; red, putative radical species.

of the nature of the various species observed in our crystals after pyruvate soaking, the stereochemistry of its binding in PFOR requires the displacement of the thiazolium ring upon reaction.

Discussion

Although crystallographic models of the oxygen-inhibited enzyme were obtained at various pH values, only the PFOR-pyruvate structure solved at pH 6.0 is reported here because it is the one that yielded the clearest electron density for the substituted ThDP. The only observed modification of the cofactor that could explain the loss of enzymatic activity is the electron density peak close to N4′ of the cofactor's aminopyrimidine ring (Figure 2). Modification of N4′ would be consistent with loss of catalytic activity because this atom is most likely involved in both deprotonation of C2 from the thiazolium ring and protonation of the carbonyl oxygen of pyruvate prior to decarboxylation. Stereochemically, the overall density is compatible with an oxime species resulting from the N-hydroxylation of the imine ThDP tautomer through reaction with O_2. As this reaction requires electrons and no external reductant was added to the medium, it is necessary to invoke limited pyruvate decarboxylation by a small fraction of active enzyme under aerobic conditions. Radical formation and subsequent radical decay would furnish two electrons per pyruvate decarboxylation (Furdui and Ragsdale, 2002). Unfortunately, we have not been able to determine the mass of the putatively modified ThDP cofactor using spectrometric methods due to fragmentation of the cofactor during the experiment. To what extent our observations apply to solution conditions remains to be determined. For instance, Williams and coworkers (Williams et al., 1990) reported a similar inhibition of the PFOR from *T. vaginalis* in the presence of oxygen-saturated buffer. However, they proposed the formation of a ThDP thiazolone species as a basis for the loss of catalytic activity, a hypothesis that is not supported by our crystal structure. Furthermore, we have been unable to fully reproduce their reported vanishing of inhibition by substrate excess in our own solution studies using the *D. africanus* PFOR (Table 1).

By taking advantage of the sluggish activity of the crystallized enzyme at acidic pHs (Figure 4), as compared to the much faster expected rate of pyruvate diffusion inside the crystal, it has been possible to synchronize the decarboxylation reaction. First, we determined the structure of a productive pyruvate-PFOR complex after a 15 min soak with the substrate followed by flash cooling in liquid propane inside a glove box. The t_{15} structure shows the orientation of pyruvate prior to any significant decarboxylation by PFOR (Figure 3, panel 2). The substrate binds with its C2α 3.6 Å away from the nucleophilic ThDP C2 carbanion and confirms our deduction based on the putative free-radical structure (Chabrière et al., 2001) that although the thiazolium ring of ThDP moves significantly to attack C2α, there are only minor adjustments in atomic positions when the binding of substrate and products are compared (Figure 5).

An omit map was also calculated using data collected from a crystal soaked anaerobically for 40 min in the pyruvate-containing solution. The t_{40} map displays electron density that can be best interpreted as corresponding to the 2-(2-hydroxypropionyl)ethyl ThDP tetrahedral intermediate (Figure 3, panel 3). Because at this resolution one could argue that the omit map may represent a mixture of reacted (acetyl radical) and unreacted (pyruvate) species, we resorted to an indirect way to distinguish between these two options. Because Tyr994 adopts different but well-defined orientations in both the native and radical structures (Chabrière et al., 2001), if there were a significant mixture of the two states in the crystal, the temperature factors (Bs) of its side chain would be relatively higher than in the case of either one or the other more homogeneous species. We have calculated the ratio between the average B factor for the Tyr994 side chain and the corresponding value for all the side chains of the PFOR dimer in the native t_0, free-radical, t_{15}, and t_{40} structures. The B ratios in the t_0 and free-radical forms are similar, 0.66 and 0.70, respectively, indicating a rather well-ordered but

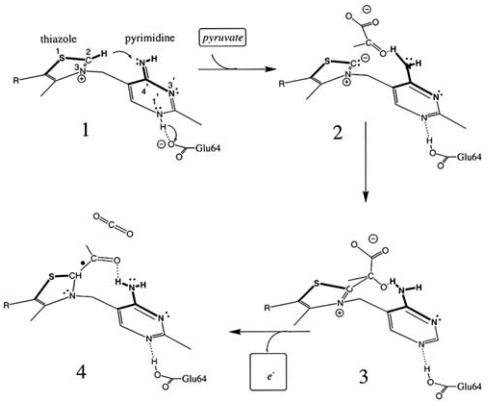

Figure 7. Catalytic Cycle Depicting the Intermediate States Reported in This Study

See Figure 3. (1) t_0; (2) t_{15}; (3) t_{40}; and (4) free-radical species. The dot over the C2-C2α signifies a one-electron bond between these two atoms. Also, note that the C2α-C2 bond between the acetyl and thiazole moieties is unusually long (Chabrière et al., 2001) and thus incompatible with enamine formation as normally postulated (see Figure 1).

differently oriented tyrosine side chain. In the t_{15} structure the equivalent value is 1.02, reflecting some heterogeneity in the conformation of Tyr994 that results from limited reaction between pyruvate and ThDP. This fact is also reflected by the shape of the electron density corresponding to the thiazolium and the orientation of Asn996, as shown in Figure 3, panel 2. More interestingly, however, the B ratio for t_{40} is 0.84 (the ratio is 0.56 for a 60 min structure; data not shown), suggesting that it corresponds to a rather homogeneous species. Furthermore, Tyr994 adopts the orientation observed in the structure of the free-radical form of PFOR that should also be expected in the tetrahedral intermediate because the cofactor moves toward the substrate to form the C2-C2α bond (Chabrière et al., 2001). In fact, refinement of t_{40} using an initial unreacted pyruvate-ThDP model shifted the thiazolium ring toward the position and conformation it adopts in the free-radical form (Figure 3, panel 4). In addition, refinement using a tetrahedral intermediate atomic model and the X-ray data from the t_{40} crystal gave an essentially featureless $[F_o - F_c]$ difference electron density map (data not shown). In pyruvate decarboxylase, the thiazolium ring of the tetrahedral intermediate was calculated to be planar (Lobell and Crout, 1996). Unexpectedly, in PFOR the electron density is not compatible with a planar thiazole ring and the concomitant π-type radical (Figure 3, panels 3 and 4). Although this issue could be expected to be solved by density function theory' calculations, our own unpublished observations indicate that the resulting models are very sensitive to the protein environment and the assigned protonation states of the ThDP. Consequently, we have not pursued these studies any further. Figure 7 summarizes the different putative intermediates identified in this study.

In order to determine the effect of X-ray exposure that might result in photoreduction of ThDP (or the $[Fe_4S_4]$ clusters), we have collected low X-ray dose data sets of pyruvate-soaked PFOR crystals and found no significant differences with the free-radical structure previously reported (Chabrière et al., 2001) (data not shown).

Superposition of ThDP cofactors in the native t_0 and putative PFOR free-radical species and the enamine intermediate of TK (Fiedler et al., 2002) indicates that the thiazolium ring of the latter is located roughly halfway between the corresponding moieties of the two PFOR species (Figure 6). Because ThDP does not move upon enamine formation in TK (Fiedler et al., 2002), there is a significant difference in the orientation of the thiazolium ring of the cofactor when this enzyme and native PFOR are compared. The TK data indicate that thiazolium ring movement is not a general requirement for C-C cleavage by ThDP. Consequently, one may wonder why there is such a significant shift of this ring upon putative radical formation in PFOR. The structure shows two unusual features: the puckering of the thiazole ring and a long, C2-C2α bond (Bellvile et al., 1985; Gauld and Radom, 1997). The question is whether the stereochemistry of the ThDP observed in our crystals could be compatible with PFOR catalysis proceeding through an enamine/α-carbanion species, as is generally accepted for the other ThDP-dependent enzymes. Our results suggest that it is not likely to be the case (Figure 7).

In conclusion, the catalytic mechanism of PFORs seems to differ in a fundamental way from that of TK, PDC, and probably from the other ThDP-dependent enzymes as well. The ThDP cofactor undergoes conformational changes in PFORs that may be unique to these enzymes.

Experimental Procedures

Crystallization

PFOR was purified as previously described (Pieulle et al., 1995). Hanging drops were prepared at 4ºC by mixing 2 μl of a 7 mg/ml protein aqueous solution with the same volume of a reservoir solution containing 10% PEG 6000, 100 mM $MgCl_2$ in either 100 mM sodium cacodylate (pH 6.0) or 100 mM Tris-HCl (pH 9.0). The drops were allowed to equilibrate 48 hr and subsequently seeded with 1 μl of a highly diluted crushed crystal suspension.

Oxygen-Mediated Inhibition of *Da* PFOR Crystals

In order to study the effect of oxygen on PFOR in the presence of substrate, both activity measurements and a crystallographic analysis were performed. For the activity assay, crystals grown at 4ºC and pH 9.0 were soaked aerobically overnight at 20ºC in an artificial mother liquor containing 50 mM pyruvate. A control experiment was carried out by soaking crystals in mother liquor without the substrate. For each condition, three crystals of similar volume (about $0.8 \times 0.06 \times 0.06$ mm^3 per crystal) were dissolved in 10 μl of 50 mM Tris-HCl buffer (pH 8.5) and transferred to a glove box. The reaction mixture containing 50 μM Tris-HCl (pH 8.5), 10 μM sodium pyruvate, 0.1 μM sodium coenzyme A, 2 μM methyl viologen, and 16 μM DTT in a final volume of 1.0 ml was incubated anaerobically at 30ºC. The reaction was started by injecting 1 μl of protein solution obtained from the dissolved crystals into the assay cuvette. Rates of methyl viologen reduction, monitored by absorbance at 604 nm, were calculated using an absorption coefficient of 13.6 mM^{-1} cm^{-1}. One unit (U) of enzyme activity was defined as the amount of PFOR that catalyzes the oxidation of 1 μmol of pyruvate or the reduction of 2 μmol of methyl viologen per min. A similar experiment was performed to determine the inhibition of PFOR as a function of pyruvate concentration (Table 1). For the X-ray analyses, crystals were soaked in artificial mother liquor with 50 mM pyruvate and 25% (v/v) glycerol added, at several pH values and in the presence of air. Subsequently, they were mounted in cryoloops and flash-cooled using liquid nitrogen in the usual way.

Time-Resolved Studies

In order to get snapshots of the reaction between PFOR and pyruvate, crystals grown at pH 9.0 were transferred to an anaerobic glove box and soaked for different periods of time in the artificial mother liquor containing 50 mM pyruvate at pH 6.0. Enzyme activity at different pH values was determined as indicated in the previous paragraph. The crystals were then transferred to a cryoprotectant solution, obtained by adding 25% (v/v) glycerol to the mother liquor, and flash-cooled in liquid propane (Vernede and Fontecilla-Camps, 1999).

X-Ray Data Collection and Refinement

Data were collected at beamlines ID14-eh1, ID14-eh3, and BM-30 of the European Synchrotron Radiation Facility (ESRF) in Grenoble, France. Data reduction was carried out using XDS2000 (Kabsch, 2001). The structures were solved with CNS (Brunger et al., 1998) by the molecular replacement method using the atomic coordinates from the free-radical PFOR X-ray model (PDB code 1kek). Crystallographic refinement was conducted using CNS (Brunger et al., 1998) and the three-dimensional model was examined and modified using the graphics program TURBO (Roussel and Cambillaud, 1989). Refinement statistics are summarized in Table S1 in the Supplemental Data available with this article online.

Composite Data Sets

The technique of composite data sets (Berglund et al., 2002) was used to collect low X-ray dose data from an anaerobically pyruvate-soaked PFOR crystal in order to determine the possible effects of X-ray exposure on the conformation of ThDP. Five subsets of 20 images, corresponding to 20° each, were collected at 100 μm intervals by translating the crystal along the rotating axis at the ID14-eh1 beamline of the ESRF (16-bunch mode) with an exposure time of 30 s per image. A full data set was generated by merging these subsets with XDS2000 (Kabsch, 2001). The structure was solved as described above.

Supplemental Data

Supplemental Data include one table and can be found with this article online at http://www.structure.org/cgi/content/full/14/2/217/DC1/.

Acknowledgments

The help of the staff from beamlines ID14-eh1, ID14-eh3, ID29, and BM-30 of the European Synchrotron Radiation Facility in Grenoble, France, is greatly appreciated. We are grateful to Dominique Housset for helpful discussions.

Received: July 1, 2005
Revised: September 30, 2005
Accepted: October 4, 2005
Published: February 10, 2006

References

Bellvile, D.J., Pabon, R.A., and Bauld, N.L. (1985). Long bonds in cation radicals of vicinally difunctional molecules. J. Am. Chem. Soc. *107*, 4978–4979.

Berglund, G.I., Carlsson, G.H., Smith, A.T., Szoke, H., Henriksen, A., and Hajdu, J. (2002). The catalytic pathway of horseradish peroxidase at high resolution. Nature *417*, 463–468.

Breslow, R. (1962). The mechanism of thiamine action: predictions from model experiments. Ann. N Y Acad. Sci. *98*, 445–452.

Brunger, A.T., Adams, P.D., Clore, G.M., DeLano, W.L., Gros, P., Grosse-Kunstleve, R.W., Jiang, J.S., Kuszewski, J., Nilges, M., Pannu, N.S., et al. (1998). Crystallography & NMR system: a new software suite for macromolecular structure determination. Acta Crystallogr. D Biol. Crystallogr. *54*, 905–921.

Cammack, R., Kersher, L., and Oesterhelt, D. (1980). A stable free radical intermediate in the reaction of 2-oxoacid: ferredoxin oxidoreductase of *Halobium halobacterium*. FEBS Lett. *118*, 271–273.

Chabrière, E., Charon, M.H., Volbeda, A., Pieulle, L., Hatchikian, E.C., and Fontecilla-Camps, J.C. (1999). Crystal structures of the key anaerobic enzyme pyruvate:ferredoxin oxidoreductase, free and in complex with pyruvate. Nat. Struct. Biol. *6*, 182–190.

Chabrière, E., Vernede, X., Guigliarelli, B., Charon, M.H., Hatchikian, E.C., and Fontecilla-Camps, J.C. (2001). Crystal structure of the free radical intermediate of pyruvate:ferredoxin oxidoreductase. Science *294*, 2559–2563.

Evans, M.C., Buchanan, B.B., and Arnon, D.I. (1966). A new ferredoxin-dependent carbon reduction cycle in a photosynthetic bacterium. Proc. Natl. Acad. Sci. USA *55*, 928–934.

Fiedler, E., Thorell, S., Sandalova, T., Golbik, R., Konig, S., and Schneider, G. (2002). Snapshot of a key intermediate in enzymatic thiamin catalysis: crystal structure of the α-carbanion of (α,β-dihydroxyethyl)-thiamin diphosphate in the active site of transketolase from *Saccharomyces cerevisiae*. Proc. Natl. Acad. Sci. USA *99*, 591–595.

Furdui, C., and Ragsdale, S.W. (2002). The roles of coenzyme A in the pyruvate:ferredoxin oxidoreductase reaction mechanism: rate enhancement of electron transfer from a radical intermediate to an iron-sulfur cluster. Biochemistry *41*, 9921–9937.

Gauld, J.W., and Radom, L. (1997). Accurate theoretical structures of radical cations containing unusually long bonds: the structures of $CH_3CH_2OH^{\cdot+}$, $CH_3C{\cdot}HO^+H_2$ and $C{\cdot}H_2CH_2O^+H_2$. Chem. Phys. Lett. *275*, 28–34.

Kabsch, W. (2001). Integration, scaling, space-group assignment and post refinement (chapter 11.3) and XDS (chapter 25.2.9). In International Tables for Crystallography, Volume F, Crystallography of Biological Macromolecules, M.G. Rossmann and E. Arnold, eds. (Dordrecht: Kluwer Academic Publishers).

Kerscher, L., and Oesterhelt, D. (1982). Pyruvate:ferredoxin oxidoreductase—new findings on an ancient enzyme. Trends Biochem. Sci. *7*, 371–374.

Kletzin, A., and Adams, M.W.W. (1996). Molecular and phylogenetic characterization of pyruvate and 2-ketoisovalerate ferredoxin oxidoreductases from *Pyrococcus furiosus* and pyruvate ferredoxin oxidoreductase from *Thermotoga maritima*. J. Bacteriol. *178*, 248–257.

Lobell, M., and Crout, D.H.G. (1996). Pyruvate decarboxylase: a molecular modeling study of pyruvate decarboxylation and acyloin formation. J. Am. Chem. Soc. *118*, 1867–1873.

Menon, S., and Ragsdale, S.W. (1997). Mechanism of the *Clostridium thermoaceticum* pyruvate:ferredoxin oxidoreductase: evidence for the common catalytic intermediacy of the hydroxyethylthiamine pyropyrosphate radical. Biochemistry *36*, 8484–8494.

Patel, M.S., and Roche, T.E. (1990). Molecular biology and biochemistry of pyruvate dehydrogenase complexes. FASEB J. *4*, 3224–3233.

Pieulle, L., Guigliarelli, B., Asso, M., Dole, F., Bernadac, A., and Hatchikian, E.C. (1995). Isolation and characterization of the pyruvate-ferredoxin oxidoreductase from the sulfate-reducing bacterium *Desulfovibrio africanus*. Biochim. Biophys. Acta. *1250*, 49–59.

Reed, L.J. (1998). From lipoic acid to multi-enzyme complexes. Protein Sci. *7*, 220–224.

Roussel, A., and Cambillaud, C. (1989). Turbo-Frodo (Mountain View, CA: Silicon Graphics).

Schneider, G., and Lindqvist, Y. (1998). Crystallography and mutagenesis of transketolase: mechanistic implications for enzymatic thiamin catalysis. Biochim. Biophys. Acta *1385*, 387–398.

Schütz, A., Golbik, R., König, S., Hübner, G., and Tittman, K. (2005). Intermediates and transition states in thiamin diphosphate-dependent decarboxylases. A kinetic and NMR study on wild-type indolepyruvate decarboxylase and variants using indolepyruvate, benzoyl formate, and pyruvate as substrates. Biochemistry *44*, 6164–6179.

Tersteegen, A., Linder, D., Thauer, R.K., and Hedderich, R. (1997). Structures and functions of four anabolic 2-oxoacid oxidoreductases in *Methanobacterium thermoautotrophicum*. Eur. J. Biochem. *242*, 862–868.

Vernede, X., and Fontecilla-Camps, J.C. (1999). A method to stabilize reduced and/or gas-treated protein crystals by flash cooling under a controlled atmosphere. J. Appl. Crystallogr. *32*, 505–509.

Williams, K.P., Leadly, P.F., and Lowe, P.N. (1990). Inhibition of pyruvate:ferredoxin oxidoreductase from *Trichomonas vaginalis* by pyruvate and its analogues. Biochem. J. *268*, 69–75.

Zhang, Q., Iwasaki, T., Wakagi, T., and Oshima, T. (1996). 2-oxoacid:ferredoxin oxidoreductase from the thermoacidophilic archeon, *Sulfolobus* sp. strain 7. J. Biochem. (Tokyo) *120*, 587–599.

Accession Numbers

Atomic coordinates and structure factors have been deposited in the Protein Data Bank with accession codes 2c3u for the oxygen-inhibited form, 2c3m for the native form, 2c3o for the t_{15} pyruvate-PFOR complex, 2c3p for the t_{40} pyruvate-PFOR complex, and 2c3y for the free-radical species.